The White Pine Controlled Collapse Experiment

Scott Phillips
D. Craig Pearson
C.L. Edwards
Brian W. Stump

Earth and Environmental Sciences Division
Los Alamos National Laboratory
University of California
Los Alamos, NM 87545

November 25, 1996

LAUR-96-2642

The White Pine Controlled Collapse Experiment

Summary

We recorded an explosively induced, 320 m deep, mine collapse and subsequent aftershocks at White Pine, MI, using a 2 km aperture array of 12, three-component surface stations. The explosions prior to the collapse produced little seismic energy. The collapse itself generated strong free-fall and slap-down phases. Free-fall time was shorter than expected given the room height, indicating height reduction by rubble generated during pillar blasting. Coda lengths of regional seismograms gave an upper-bound magnitude of 3.1, leading to upper-bound estimates of displaced mass of $5.6X10^8$ kg and thickness of 11 m. Compressional (P) waves observed regionally included emergent free-fall phases followed by impulsive, upward, slap-down phases.

The largest aftershocks generated amplitudes two orders of magnitude smaller than those of the collapse. Occurrence rate fell off quickly, 90% of the aftershocks happened in the first 4 hours following collapse. These observations demonstrated that deploying instruments to refine regional locations for verification/discrimination purposes would be difficult. After calibration using a pillar shot and two well-recorded microearthquakes, we obtained 135 high-quality aftershock locations. The aftershock zone was under 100 m thick, bottoming at mine level, peaking over 200 m beneath the surface and indicating no collapse-related deformation extending into the shallow aquifer. Aftershocks fell away from the unmined faces of the collapsed panel and concentrated along the open, western edge where the shallowest aftershocks were observed. This asymmetrical distribution was consistent with relatively low stresses measured in the first row of intact pillars.

Participants

White Pine: Daniel St. Don, Steve Brooks.
LANL: Craig Pearson, C.L. Edwards, Brian Stump, Diane Baker, Roy Boyd, Scott Phillips, Hans Hartse, Keith Kihara, Keith Dalrymple.

Experimental Purpose

We collected seismic data during a controlled, explosively induced mine collapse at White Pine, MI to address seismic discrimination, environmental monitoring and mine engineering issues. Near-source recordings of the ground motion during the collapse will lead to a firmer basis for discriminating between unusual mine collapses, underground nuclear tests and natural earthquakes. A 1988 White Pine collapse was assigned a magnitude of 3.6, large enough to be of concern under the terms of the Comprehensive Test Ban Treaty. Collapse recordings should indicate details such as displaced mass and "time-of-flight" that may be relevant to collapse design as well as to discrimination. The study of aftershocks will define the subsurface volume surrounding the collapse where seismic deformation continued to occur because of the redistribution of stresses. Aftershocks shallow enough to reach the near-surface aquifer will indicate potential environmental problems. The extent of the aftershock zone will have important implications for collapse design. In addition, aftershocks may help to locate a mine collapse or discriminate between a mine collapse and an underground nuclear test.

Setting

The White Pine Mine is located near Lake Superior on the Upper Peninsula of Michigan in the vicinity of the town of White Pine, Michigan (Figure 1). The southern shore of Lake Superior is approximately 9 kilometers to the north of the townsite. The area is sparsely populated. Tourism, harvesting of pulp wood for paper milling and copper mining are the major industries in the area.

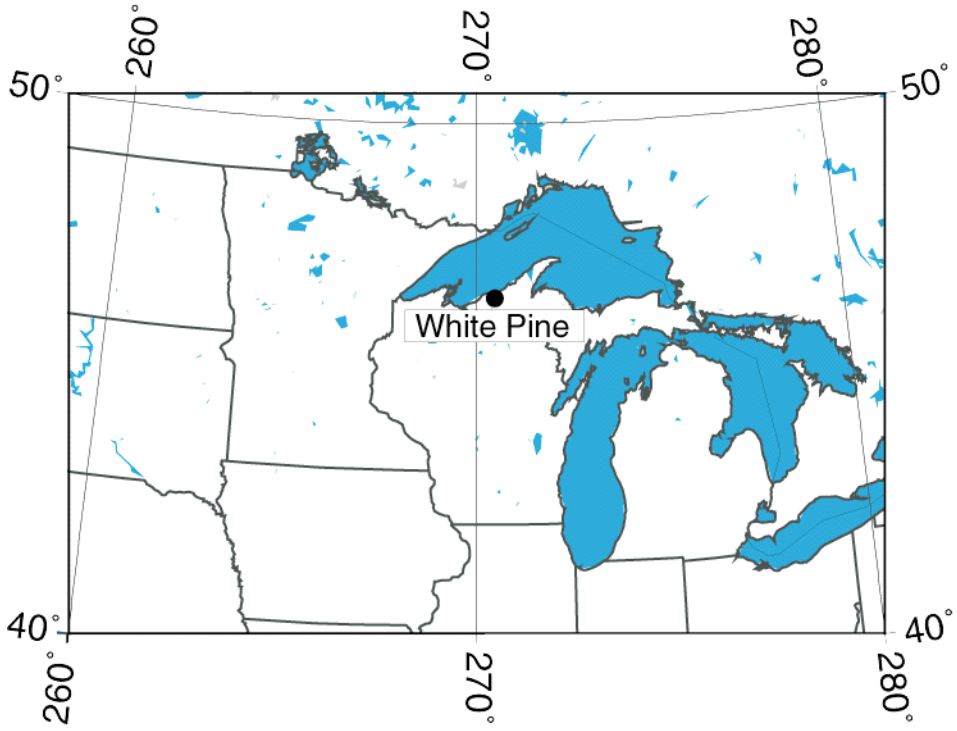

Figure 1. Location of the White Pine mine, Upper Peninsula, Michigan.

The terrain varies from relatively flat, lake-shore regions incised with small rivers at elevations ranging from 600 to 1100 feet above sea level to semi-mountainous to the west and south with elevations ranging from 1100 to 1800 feet. Vegetation is dense and poses a high degree of hardship for deployment of seismic equipment. Weather conditions are also extreme with high temperatures and humidity in the summer and very low temperatures and large amounts of snow pack in the winter.

The primary mineral being mined is copper which was hydrothermally emplaced into folded and faulted, low grade metamorphosed, meta-sandstones and meta-shales of Cambrian age. Figure 2 shows a map view of a model of the local geological structure at the horizon of the ore body. The well known White Pine Fault is a large normal fault that strikes at 131 degrees (southeast) and dips steeply at 221 degrees (southwest) and is evident in the lower left quadrant of Figure 2. The White Pine fault dissects a large anticlinal structure which plunges at approximately 10 degrees along a trend of approximately 130 degrees (southeast).

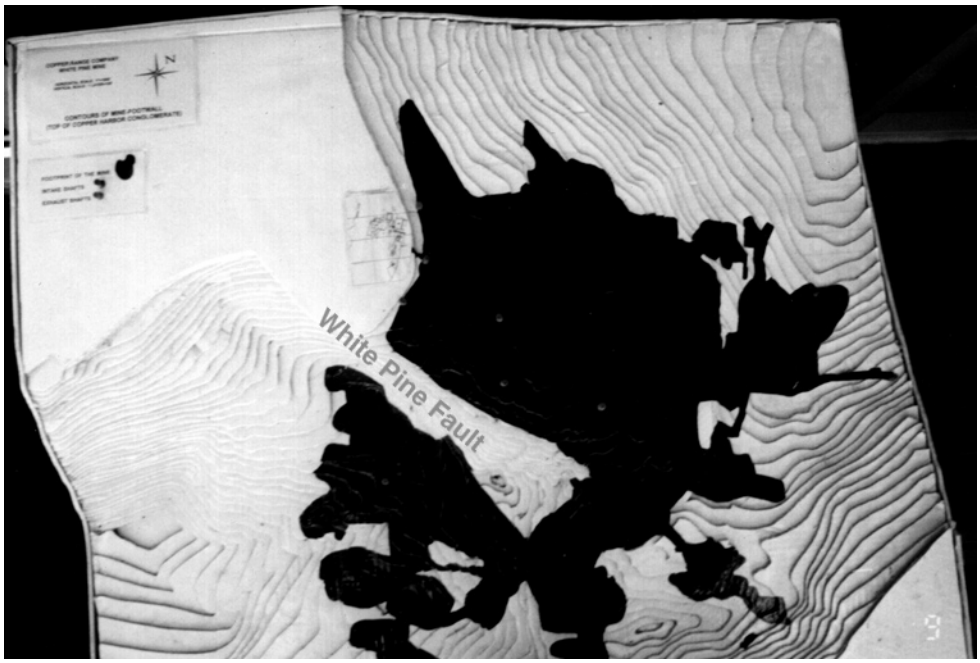

Figure 2. Three-dimensional model of the White Pine mine, contour interval 100 ft.

The underground workings at the mine, shown as a map view in Figure 3, are extensive, with rough dimensions of 8 km by 9 km. Historically, portions of the mine have collapsed "naturally" and are denoted by dark black areas in the figure. The naturally collapsed area in the north-central portion of the mine has collapsed slowly over a period of many years. The collapsed area south west of the White Pine Fault failed catastrophically, producing a locally felt earthquake and extensive damage to underground mine structures (St. Don, personal communication 1995).

Recently discontinued operations at the mine relied on ore removal by the room and pillar mining technique with subsequent movement of the ore to the surface for processing. A number of economic factors have led to the decision to discontinue the room and pillar

operation and to begin investigation into the effectiveness of pillar rubblization and in-situ leaching of the ore body remaining in the pillars. The controlled collapse documented here is the first of its type in the White Pine Mine.

A layer of glacial till, 10 to 20 m thick covers the surface at White Pine. The top of the water table is shallow, 1-2 m beneath the surface. Pre-Cambrian bedrock, consisting of Freda sandstone, Nonsuch shale and Copper Harbor conglomerate underlies the glacial till surface material. The mine follows the shale-conglomerate interface at a depth of 320 m in our study area. The depth to this interface varies laterally, as shown in the three-dimensional model of the mine (Figure 2). These geological structures will be important to consider when calibrating the subsurface propagation times for microearthquake location purposes.

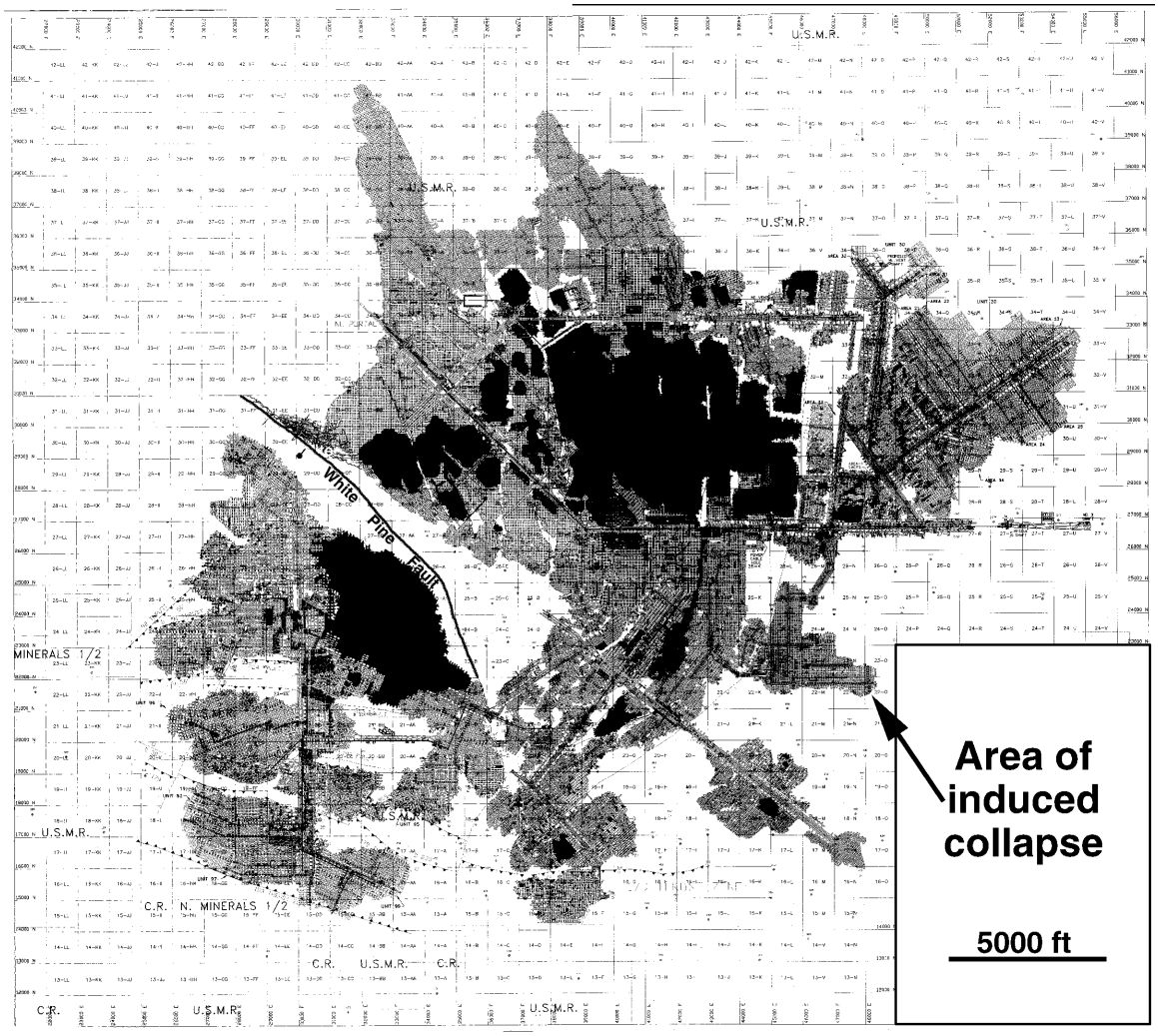

Figure 3. Plan view of underground workings at White Pine. Hachured areas indicate room-and-pillar mined areas while black indicates failed-pillar areas. The failed area outlined in the lower left quadrant on the hanging wall of the White Pine Fault was the catastrophic event of January 1988.

The Controlled Mine Collapse

The initial, pillar-removal operation was conducted on September 3, 1995 at 5:39 PM local time (246:21:39:38 UTM). Seventy-two (72) pillars with average dimensions of 6.1 m by 12.2 m were loaded with an average of 1,807 lb. of explosive per pillar for a total explosive source of 130,068 lb. A millisecond delay firing pattern, 325 milliseconds in length, was used to minimize vibration effects at the surface and propagate the collapse toward the unmined faces as shown in Figure 4. Note that this preliminary test event was designed to be only 1/4 the size of future, full-scale panel blasts (St. Don, 1995).

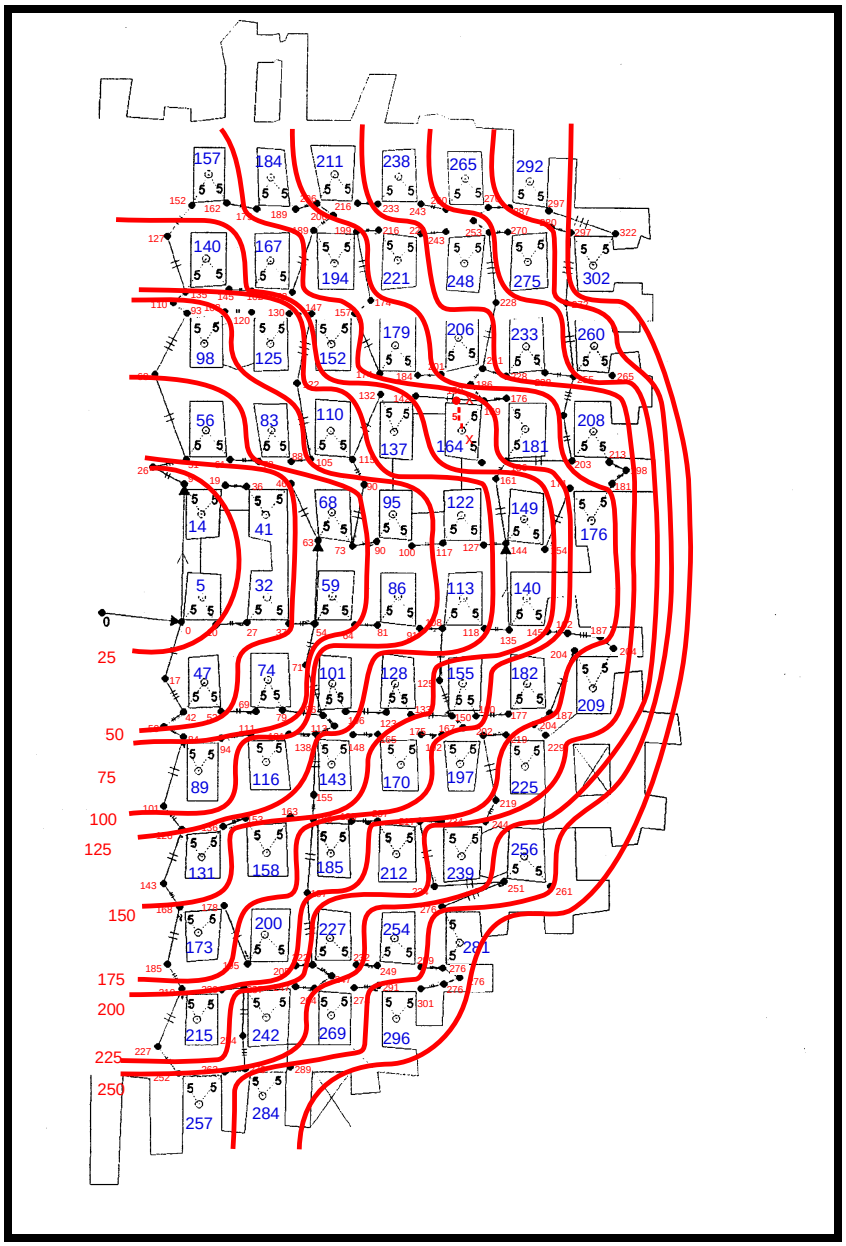

Figure 4. Map view of collapsed panel showing details of the pillar rubblization blast. Contours represent time delays in milliseconds.

Seismic Data Acquisition

Prior to the shot, LANL personnel fielded a three-component seismic network designed to characterize near-source wave propagation effects and to determine locations of aftershocks associated with stress redistribution following the explosive pillar removal. A map of the seismic network is shown in Figure 5 while pertinent station location information relative the ground zero station are listed in Table 1. Stations were located using handheld GPS receivers. The network was designed primarily to determine the extent to which chimneying of the overlying rock propagated following the pillar removal. The level at which the explosion occurred is approximately 320 m below the surface.

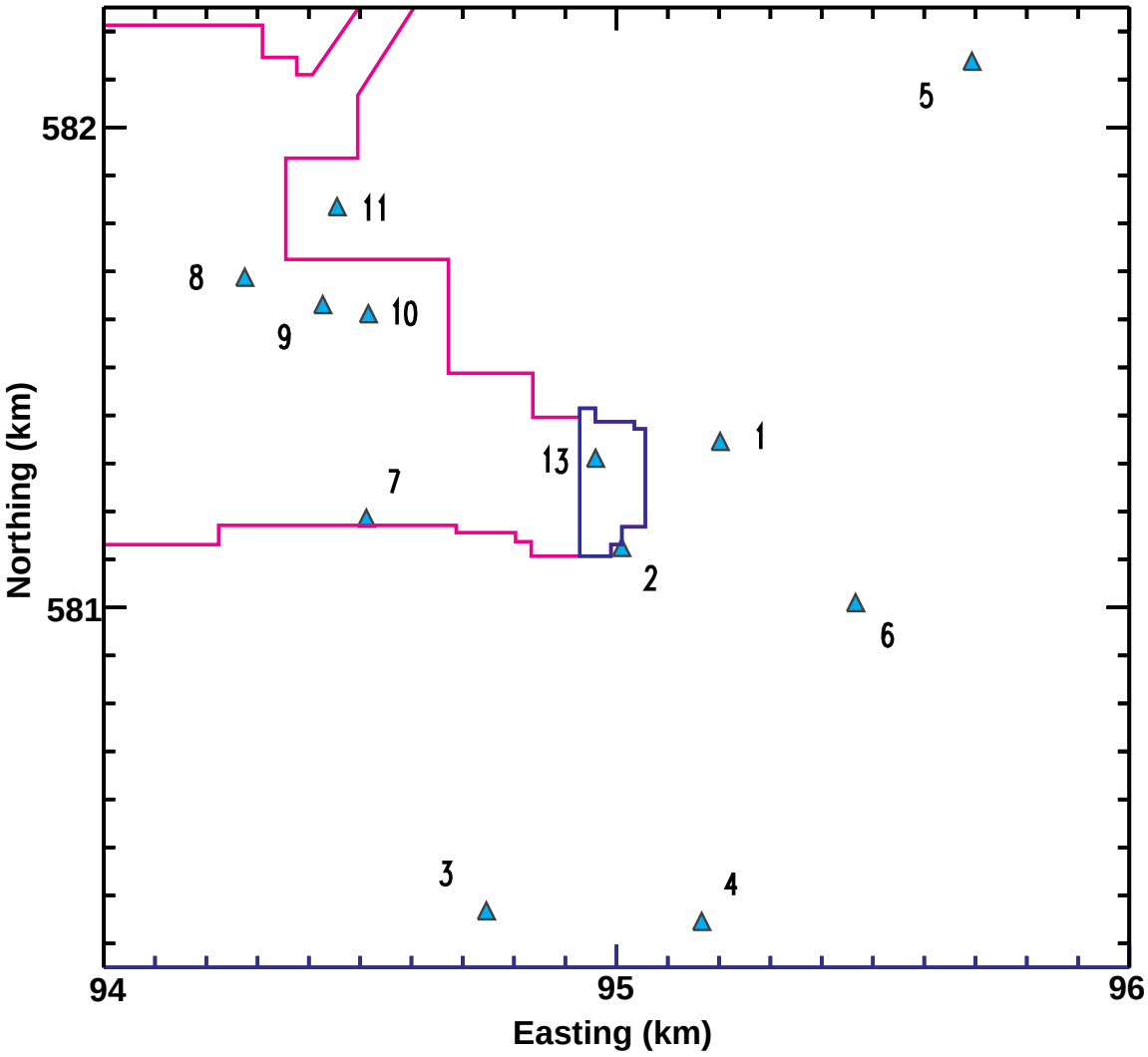

Figure 5. Map of three-component station locations. The pink line represents the mine face, room-and-pillar mined areas fall to the northwest. The purple line indicates the collapsed panel. Easting and northing are Michigan state coordinates.

Table 1. White Pine Stations and Station Corrections.

Station Number	Northing km	Easting km	P Correct ms	S Correct ms
1	581.346	95.202	10	4
2	581.125	95.010	15	27
3	580.368	94.746	-4	-2
4	580.346	95.166	4	1
5	582.138	95.693	4	-23
6	581.010	95.466	-18	-41
7	581.186	94.512	2	-9
8	581.688	94.275	7	-7
9	581.631	94.427	9	-13
10	581.612	94.516	11	-15
11	581.835	94.455	10	-17
13	581.311	94.959	20	29

Twelve stations of the seismic network were distributed in azimuth and range out to approximately 1000 m (stations 1-11 and 13). A thirteenth seismic station was located at a range of approximately 5 km (station 12), primarily to record the electrical shot break signal and secondarily to characterize the wave-field as it propagated away from the source region. Each station was instrumented with a six channel, Refraction Technology Model 72A-08 data logger which was continuously locked to GPS broadcast timing signals for adequate timing accuracy. Three-component, 1 Hz, Mark Products Model L4-3C geophones were fielded at each station and a three-component, Terra Tech SSA-302 accelerometer was fielded at station 2. All stations were programmed to record event triggered data using a STA/LTA algorithm with the exception of station 13 (near-surface ground zero) which recorded continuously. The STA length was 0.1 s, LTA, 10 s, with ratio thresholds of 6 to 8 depending on the station. All channels were initially programmed to record with unity gain to avoid saturation. Stations 2 and 13 were digitized at 250 samples/s, other stations at 500 samples/s. The dataloggers applied low-pass, anti-aliasing filters with corner frequencies 95% of the Nyquist. In addition to the seismic stations, a Hi-8 video camera was deployed at station 13 to document surface motion and acoustic signals.

All seismic stations triggered on the induced collapse event and continued to trigger during the aftershock sequence (Figure 6a, b). The seismic traces recorded at station 12 were contaminated with strong 60 Hz noise induced by ground loop with the electrical firing system. Because there was no noticeable expression of the collapse at the detonation point, the video camera deployed at station 13 (near ground zero) was recovered within 1 hour of the event to verify that the explosives had detonated and the collapse had occurred. During recovery of the camera, B. Stump noted that aftershocks could be felt and heard at station 13.

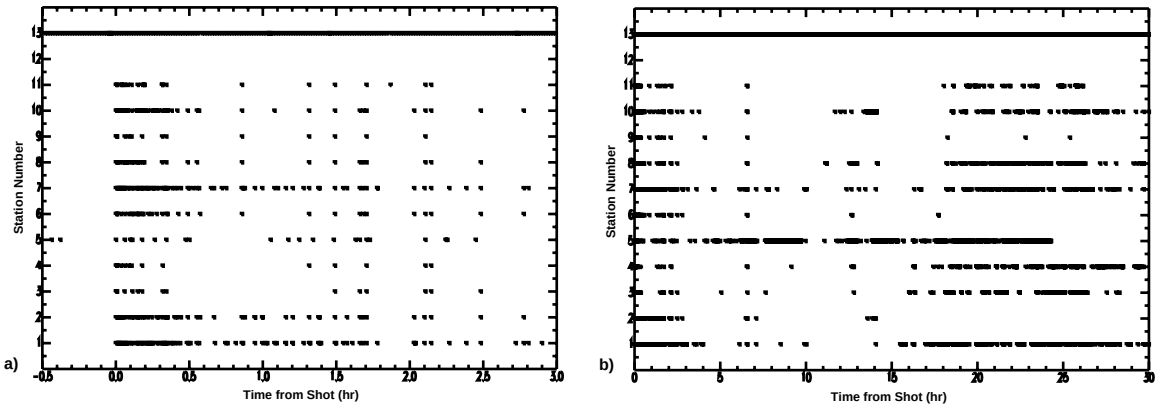

Figure 6. Event triggers at each station for a) 3 hours and b) 30 hours following the collapse.

Data acquisition parameters were changed approximately 12 to 14 hours following the main collapse by increasing the pre-amplifier gain. Stations at 2 to 3 depth of burial surface ranges were increased to a gain of x32 and stations at less than 2 depths of burial were increased to a gain of x8. Trigger rates increased at this point (Figure 6b). Data acquisition continued for approximately 36 to 40 hours following the main collapse.

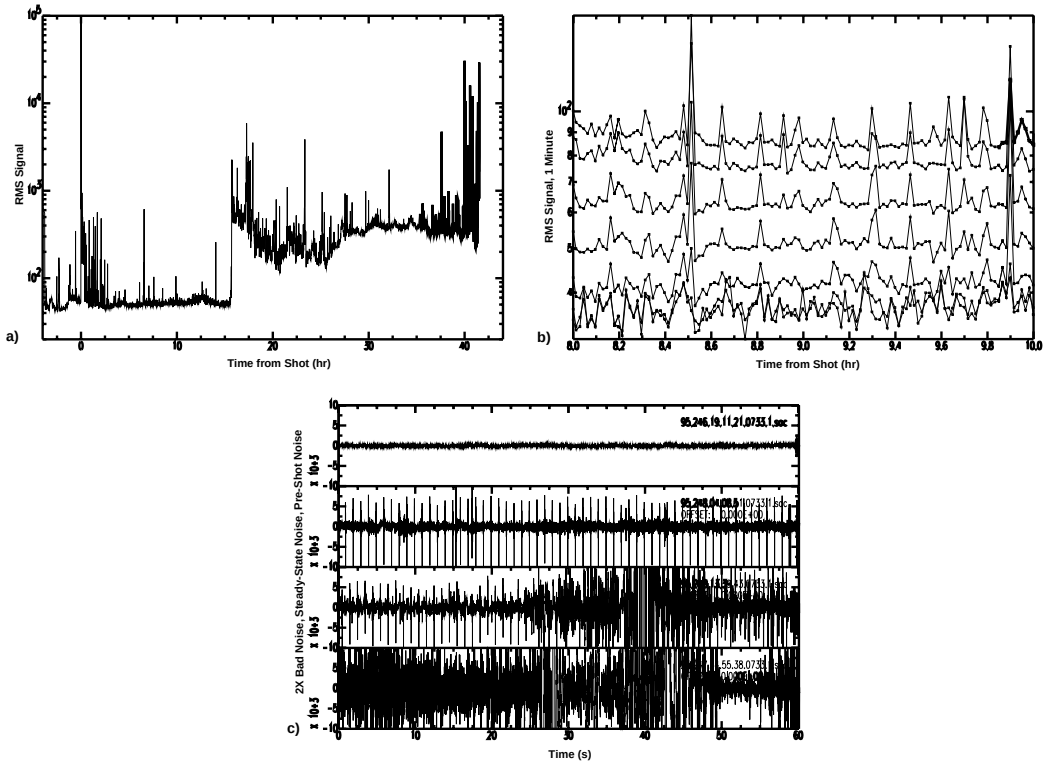

Figure 7. Vertical-component noise recorded at station 13: a) RMS 8 to 16 Hz noise for 1 minute intervals throughout experiment (note gain change at 15 hours), b) blow up of RMS results, bands 1-2 Hz to >64 Hz showing 10-minute spikes, and c) extreme quiet and noisy records showing 1-second spikes and ground motion from passing wildlife.

Network-averaged, RMS, vertical-component noise was $8X10^{-5}$ cm/s for a one second interval directly preceding the shot. Little noise was found to be associated with the mine ventilation system (Figure 7a). Transient signals from wildlife were common. The 1 second and 10 minute spikes we noticed in station 13 data may have been generated by the data recording system (Figure 7b, c).

Mine-Collapse Data

High-quality, three-component velocity seismograms of the mine collapse were acquired at each of the local stations. Figure 8 shows instrument-corrected, vertical-, radial- and transverse-component signals at all stations. At surface ground zero (station 13), the vertical component of motion was a factor of five larger than the horizontal components. At this amplification, the individual explosive sources in the pillars were not resolved but failure of the pillars was indicated by the high-frequency arrivals on the vertical component. These failure signals rode on top of a long-period signal indicating an initially upward motion associated with release of material above the working level. This was followed by strong downward motion associated with the "slap down" of the released material. Dominant motions shifted to the radial component with increasing distance from ground zero. The spectra shown in Figure 9a indicate the peaked nature of the vertical component at surface ground zero. Horizontal spectra at surface ground zero were essentially flat to 5 Hz and exhibited spectral modulation similar to the vertical component (Figure 9b).

Ground motion associated with pillar blasting was relatively small, but can be seen easily if we amplify the signal immediately preceding the collapse (Figure 10).

Regional seismograms of the induced collapse were recovered from stations at ranges from 200 to 1000 km (Figure 11). Coda lengths (150 s) indicated a magnitude (m_{bLg}) of 3.1 using a scale developed for New England (Chaplin et al., 1980). This magnitude is considered an overestimate because Lg-coda attenuation is higher in New England than in north-central US (Singh and Herrmann, 1983). P-wave signals were initially emergent, followed by a strong upward pulse, associated with the slap-down phase of the mine collapse (Figure 12a, b).

Aftershock Data

Two hours of station 13, vertical-component data starting with the mine collapse are shown in Figure 13. Event rates approach 50 per minute over the first 5 minutes and fall off to 1 to 2 per minute in two hours. Odd signals at 22 and 26 minutes are scientists approaching ground zero to check equipment. Because seismic recorders triggered independently, we gathered data segments by time (association) before identifying individual events. Identification was performed manually by displaying all available data for a given time window and choosing events that were recorded at three or more stations. 220 events were identified in this manner. The number of locatable three-station events per 6 minute interval (0.1 hour) are shown in Figure 14a, b. Event rates were highest over the first 12 minutes (7 events per minute) and dropped to 1 event per minute after 30 minutes. Over 90% occurred within 4 hours of the collapse. The remaining 10% occurred during isolated swarms of activity through the remaining 36 hours of network operation.

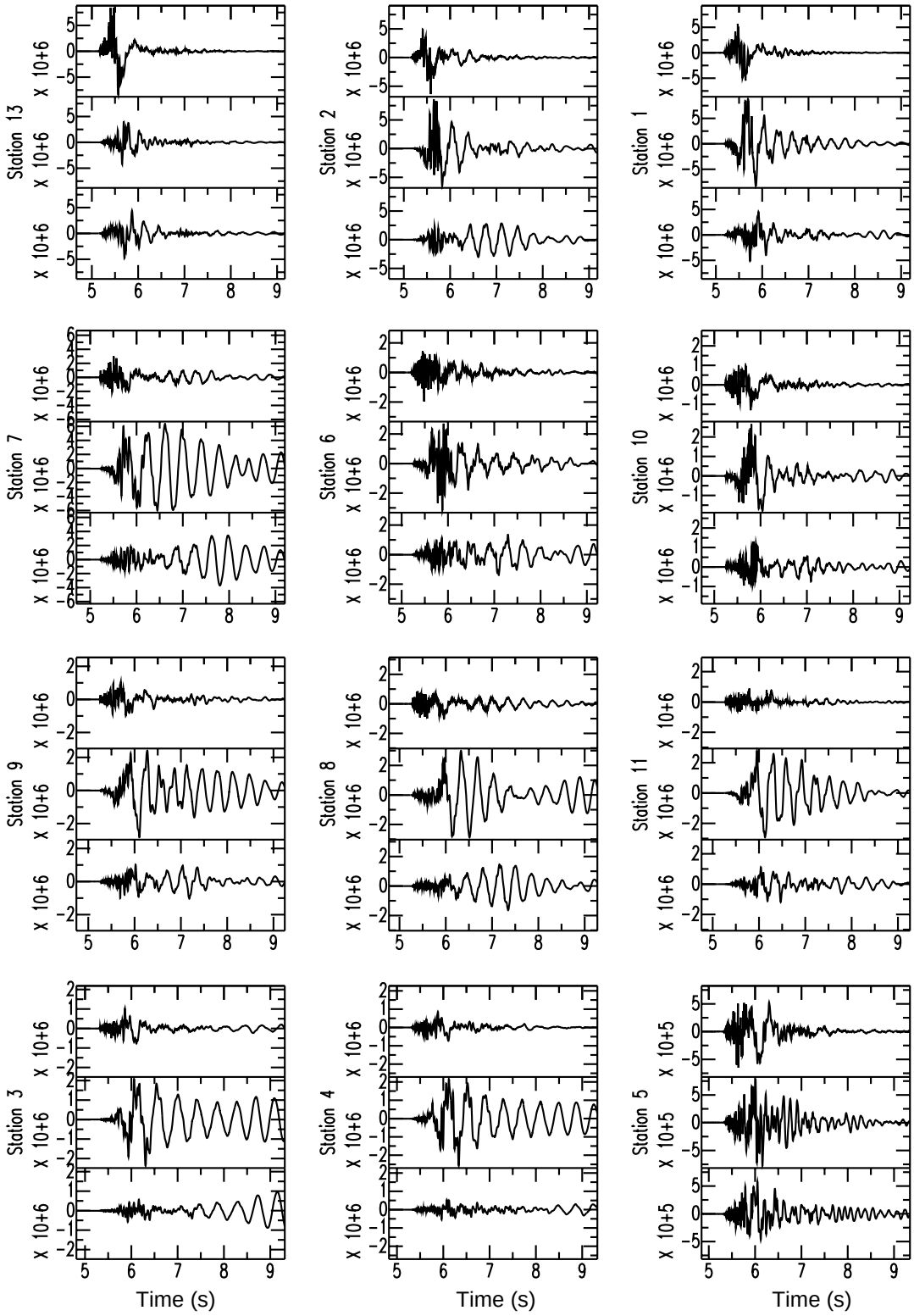

Figure 8. Vertical-, radial- and transverse-component velocity seismograms acquired during collapse. Stations are arranged in order of distance from ground zero.

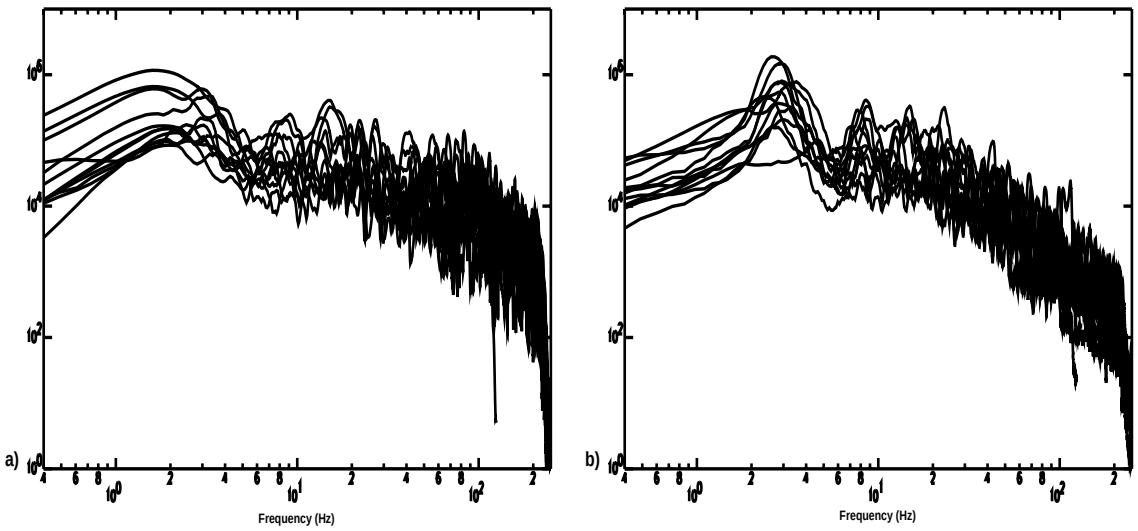

Figure 9. Spectra of velocity seismograms shown in Figure 8: a) vertical components and b) transverse components.

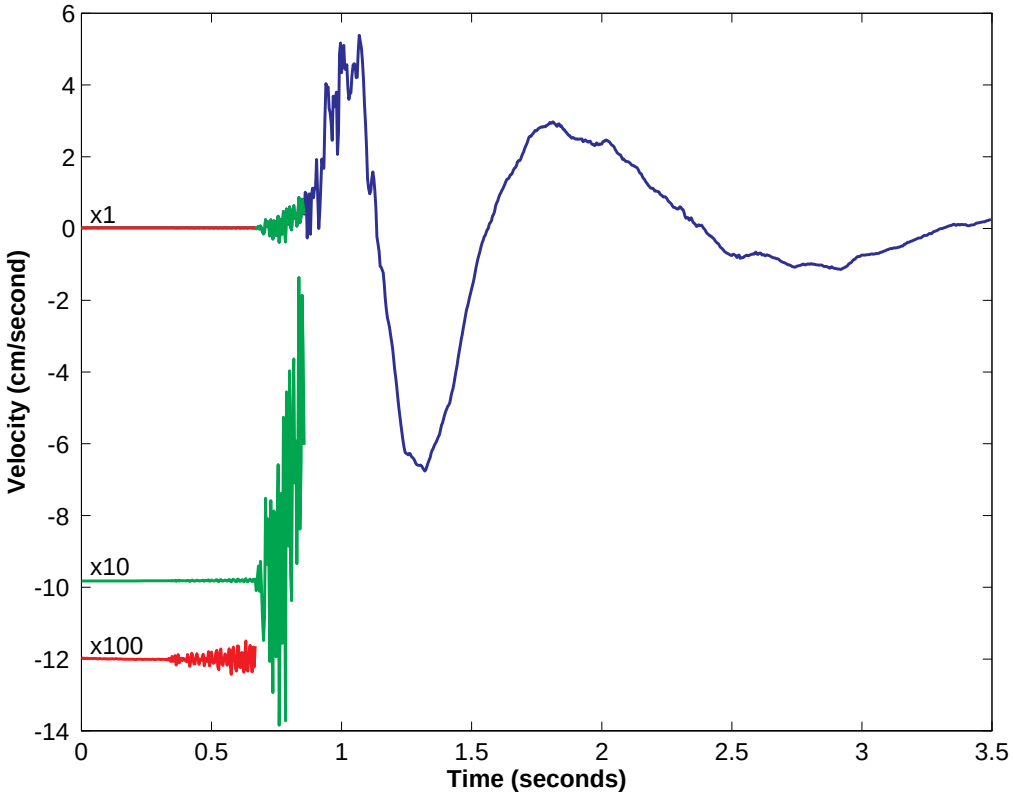

Figure 10. Vertical component velocity seismogram recorded at ground zero. The upper trace is the complete seismogram, dominated by the long period collapse. The middle and lower traces are magnified by 10 and 100 times, respectively. The green middle trace shows pillar failure and the red lower trace shows the explosions in the pillars.

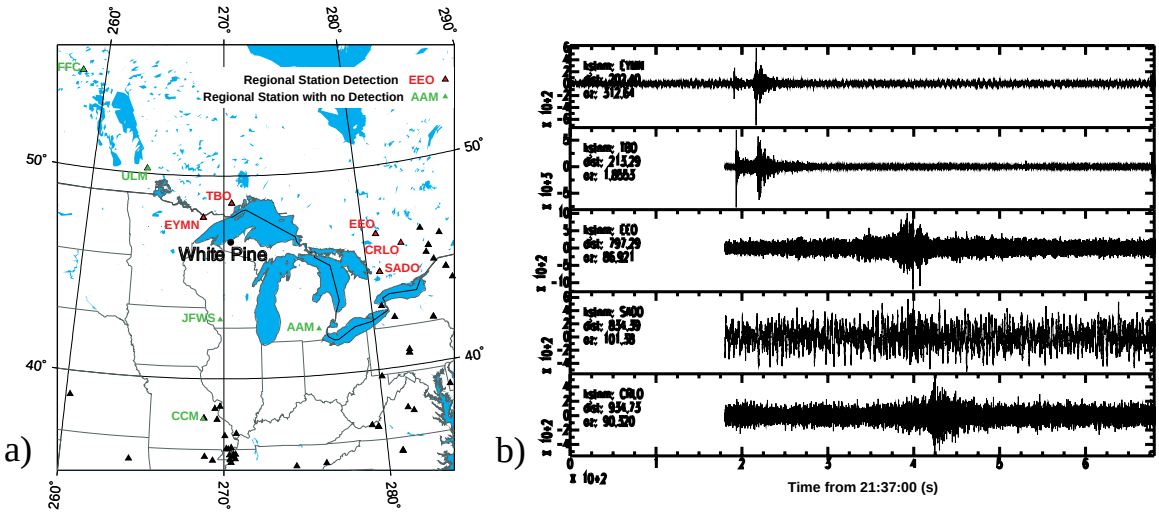

Figure 11. a) Map showing regional stations and b) vertical-component seismograms from the White Pine collapse. EYMN seismograms were high-pass filtered at 0.75 Hz.

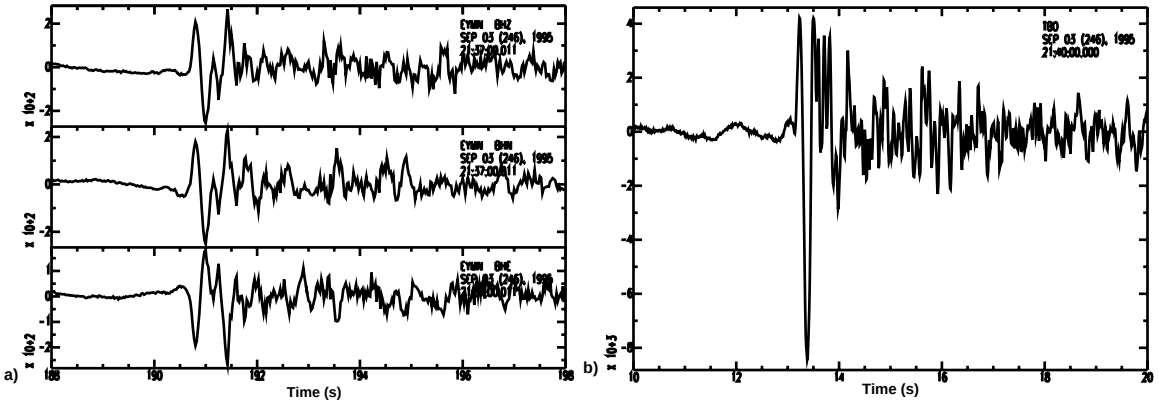

Figure 12. Regional P waveforms from the White Pine collapse observed at a) EYMN and b) TBO.

The largest of the aftershocks were more than two orders of magnitude smaller in amplitude than the collapse event. Seismograms displayed shear-slip characteristics as indicated by the large amount of radiated shear (S) energy and the presence of compressional and dilitational motions of the P wave. The number of compressional versus dilitational, high-quality first motions are plotted for each station in Figure 15. Most first motions at central stations were up, outer stations were down, suggesting thrust-type source mechanisms.

Vertical-component (P-wave) spectra show significant energy at 100 Hz, tapering to noise levels between 100 and 200 Hz (Figure 16a). Because this sample aftershock event was relatively large, the spectra indicated upper bounds on signal bandwidth. Therefore, stations with sample rates of 500 Hz recorded the full signal bandwidth. However, stations digitizing at 250 Hz missed significant signal above the anti-aliasing corner frequency,

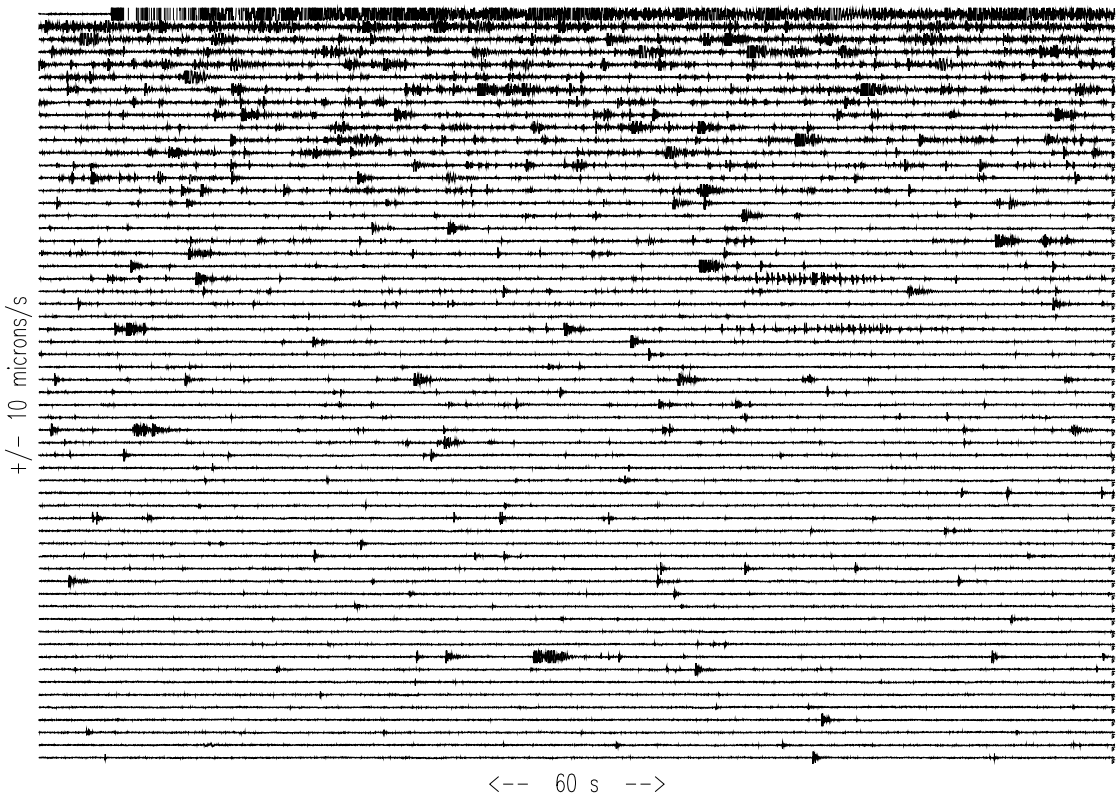

Figure 13. Station 13 vertical-component seismograms covering the first 1 hour following the collapse. The amplitude scale is fixed.

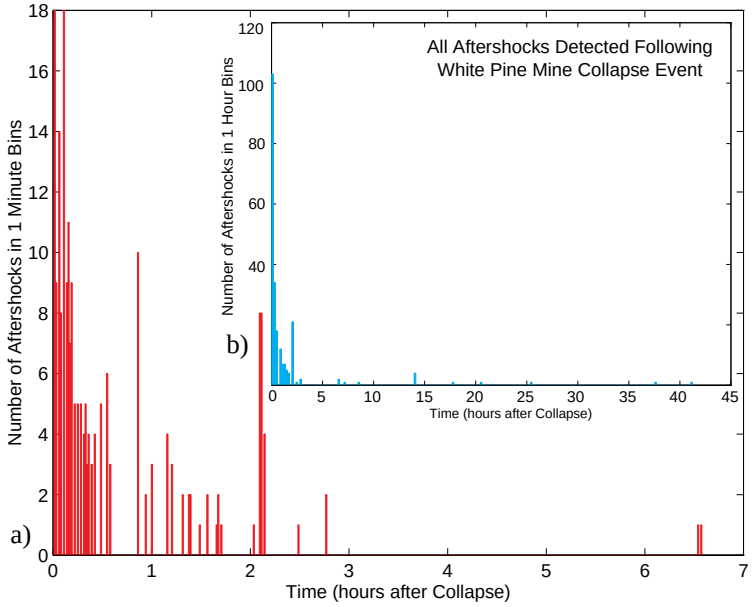

Figure 14. Number of locatable aftershocks per 6 minute interval (0.1 hour) for a) 2.8 hours and b) 45 hours following collapse.

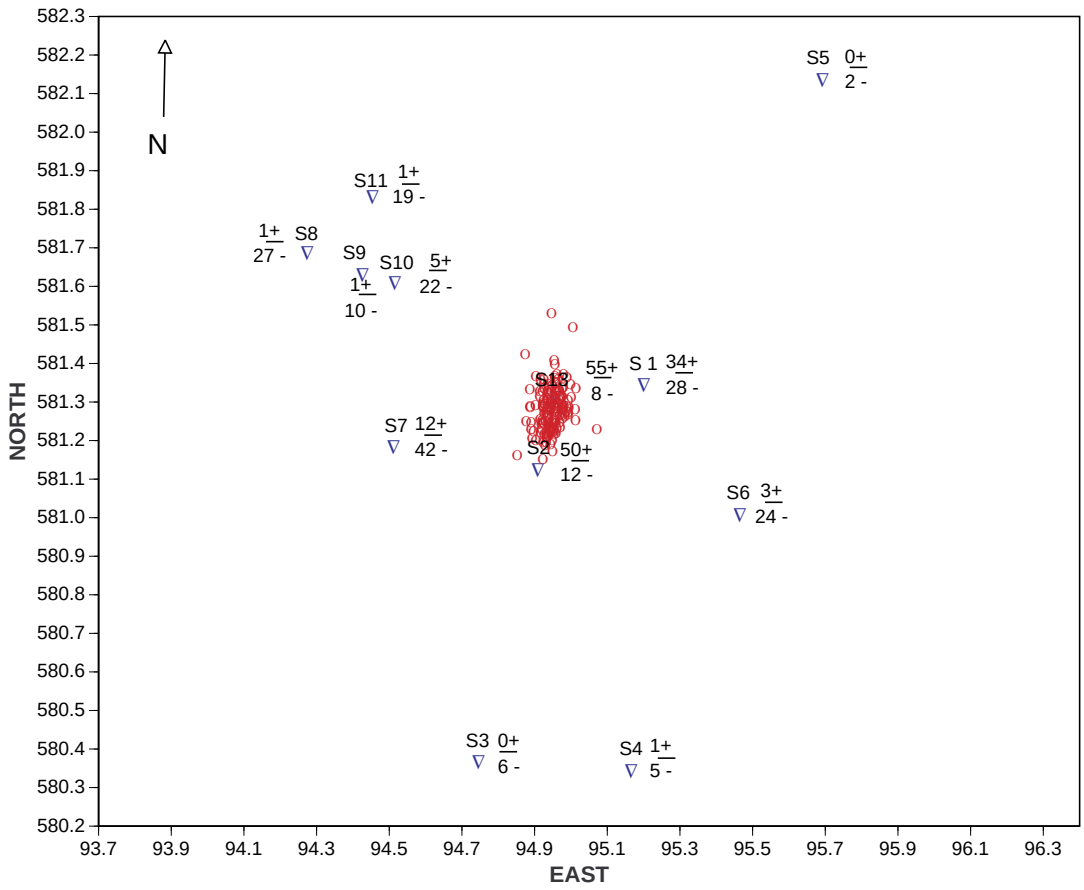

Figure 15. Number of high-quality (0 only) P-wave polarities (up/down) measured at each station.

especially for larger events. Transverse-component (horizontally polarized S-wave) spectra were relatively deficient in high frequencies, tapering to the noise at about 100 Hz (Figure 16b).

Small events often preceded larger events, by 20 ms or less, in the aftershock data set (Figure 17). We do not know if this is a true precursory phenomenon; however, it made associating P and S waves from the same event difficult, occasionally resulting in poor locations.

We also noticed unusual arrivals in the P coda at many stations, especially station 7 (Figure 18). Without modeling, we hypothesized that this was a phase converted at the interface between Nonsuch shale and Freda sandstone. Travel times of this phase varied smoothly with distance (Figure 19). If the phase can be identified, its arrival times can be used for calibration and location purposes.

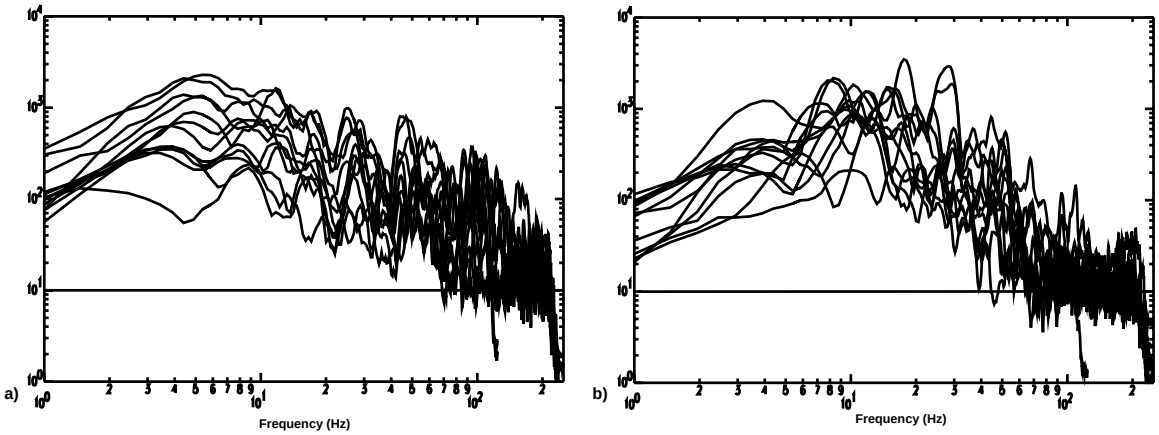

Figure 16. Aftershock velocity spectra of all records from a single event: a) vertical component and b) transverse component. Noise levels are indicated by the horizontal bar.

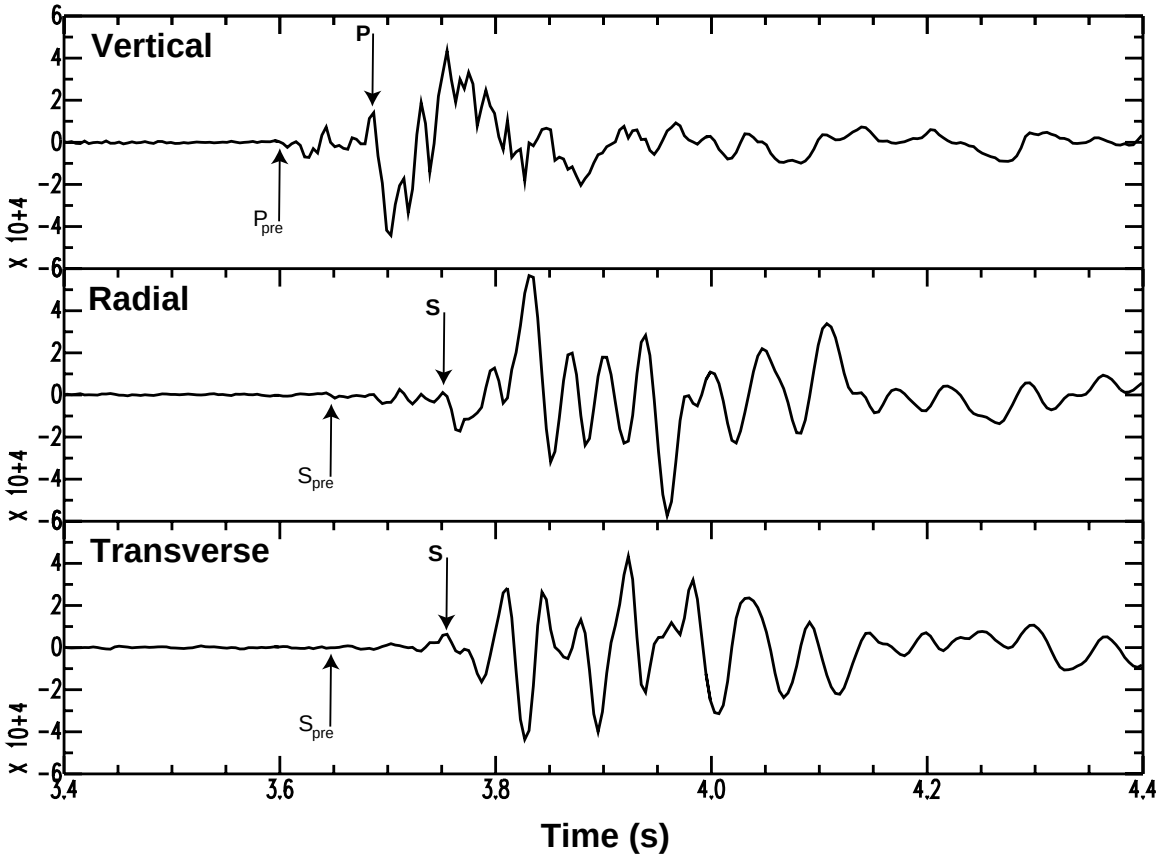

Figure 17. Aftershock accompanied by small precursor. The compressional and shear wave arrivals of the precursor are labeled as P_{pre} and S_{pre}, respectively. The compressional and shear wave arrivals of the aftershock are labeled P and S, respectively.

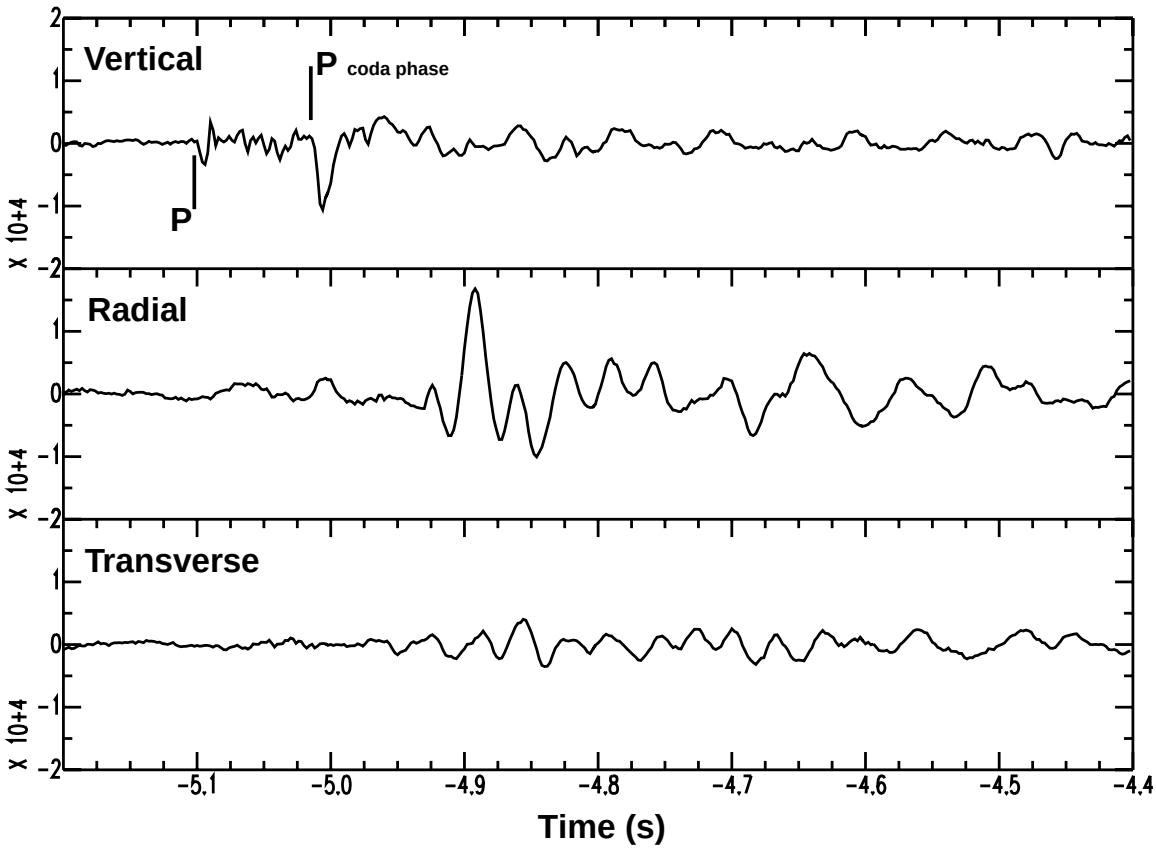

Figure 18. Aftershock seismogram from station 7 exhibiting secondary arrival in the P coda.

Aftershock Location Method

We had to calibrate the collapse area before microearthquakes could be located. Calibration consisted of creating P- and S-wave velocity models of the subsurface as well as P- and S-wave station corrections. The station corrections accounted for small-scale deviations from the velocity model that affected travel times to individual stations. To calibrate, we used P- and S-wave arrival times from two, well-recorded microearthquakes and P-wave arrival times from the earliest pillar shot at innermost stations 1, 2, 7 and 13.

We chose a layer over a half-space model of seismic velocities. The layer contained glacial till, Freda sandstone and Nonsuch shale, thickness 320 m. The half-space contained the Copper Harbor conglomerate. The half-space velocities were calculated from the moveout of P and S arrival times of the two, well-recorded microearthquakes, assuming location at ground zero, depth 320 m and refracted ray paths through the top of the half-space (Vp=5.46 km/s, Vs=3.07 km/s, Figure 20a, b). The ratio of P- and S-wave velocities was confirmed using Wadati diagrams (Vp/Vs=1.79, Figure 21a, b). The P-wave velocity in the layer was taken from two-way travel times from Geosphere reflection lines 7 and 8 (Vp=3.80 km/s; Geosphere, 1995).

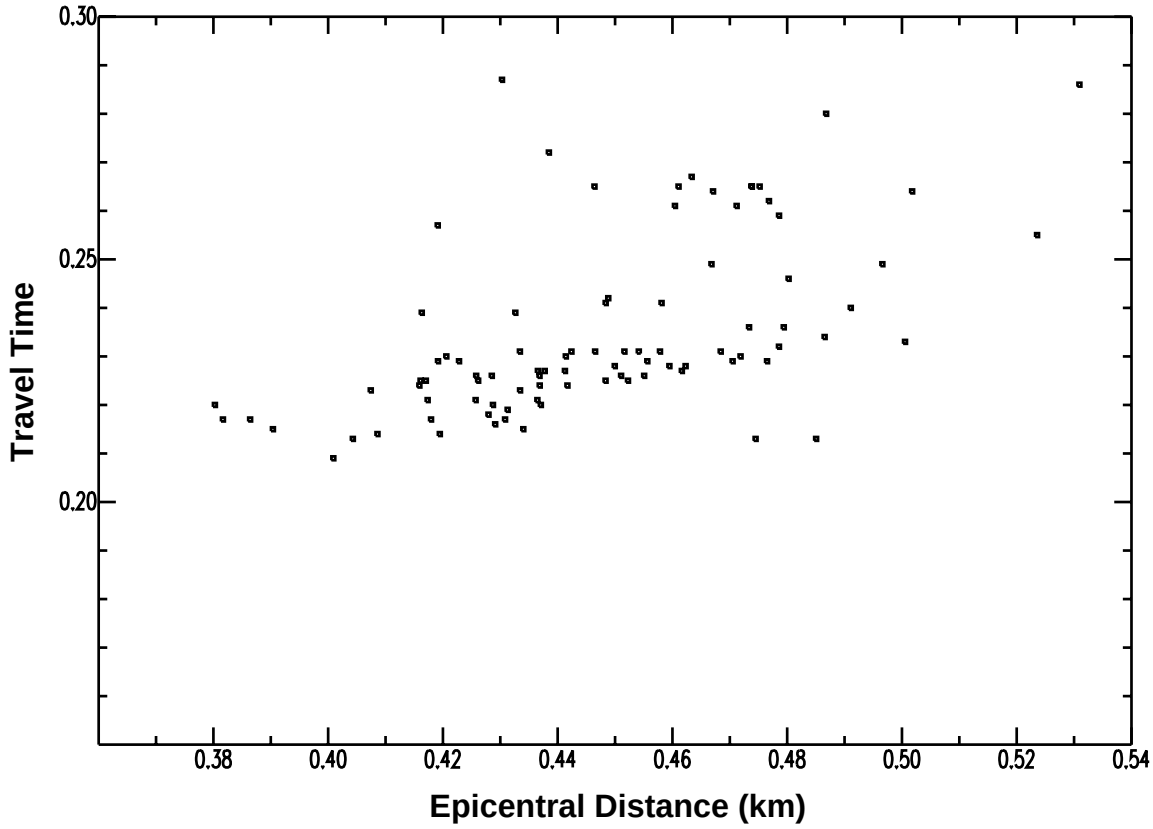

Figure 19. Station 7 secondary-arrival travel times versus epicentral distance.

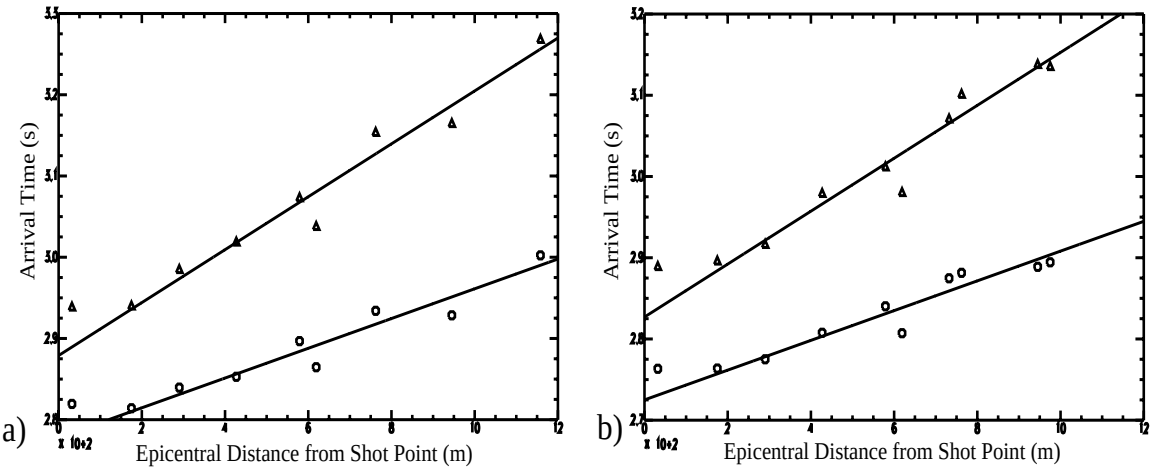

Figure 20. P and S arrival times versus epicentral distance for the two calibration aftershocks (a, b). Circles are P arrivals, triangles, S arrivals. Lines represent velocities of 5.46 (P waves) and 3.80 (S waves).

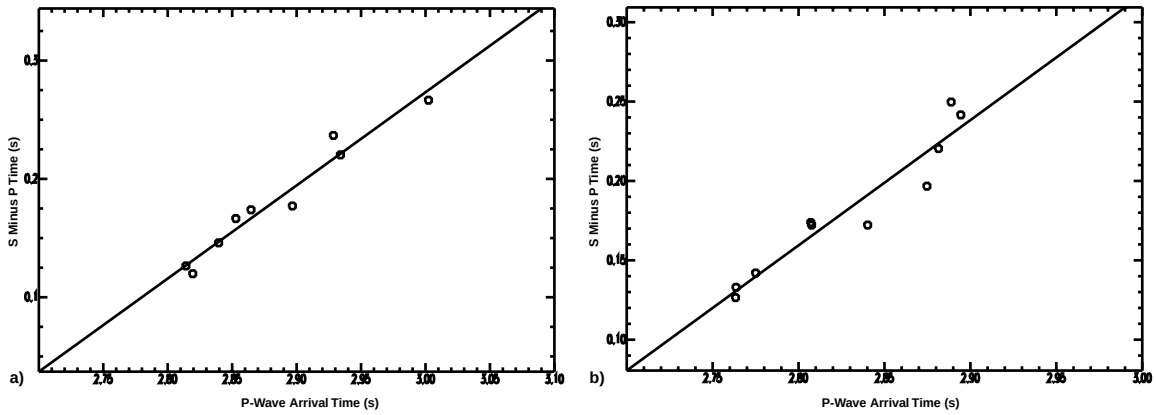

Figure 21. Wadati diagrams for the two calibration aftershocks (a, b). Lines represent a Vp/Vs ratio of 1.79.

The earliest pillar shot was best recorded at the four stations closest to ground zero (stations 1,2,7 and 13). We measured the shot initiation signal, but the actual shot was delayed by a 50 ms delay cap. Because delay cap times can vary by 10%, we could not rely on the shot initiation signal in the calibration procedure. Instead, we solved for P-wave station corrections (stations 1, 2, 7 and 13 only), using the P-wave velocity structure (above) and assuming the earliest observed phase originated at the first pillar. Following this, the two well-recorded microearthquakes were located, using P-wave arrival times and corrections at stations 1, 2, 7 and 13. We then calculated the S-wave velocity in the layer to fit S arrivals from the two microearthquakes at stations 1, 2, 7 and 13 (Vs=1.60 km/s), using locations and origin times from the previous step. The remaining P- and S-wave station corrections were calculated from arrival times of the two microearthquakes, using the complete velocity model given in Table 1. Station 9 corrections were assigned the averages of nearby stations 8, 10 and 11. The mean station correction was removed. This procedure resulted in event locations relative to the assumed shot point. We are confident in the shot-point depth, less so the shot epicenter.

The shot records were emergent as seen in Figure 22. We chose arrival times at the downswing just before the main wave train. Calibration based on these arrival times yielded microearthquake depths of 5 and 25 m above the mine level following the procedure detailed above. The other option was to choose the low-amplitude phase arriving 15 ms earlier at stations 2 and 13. When these arrivals were used, the microearthquakes located up to 200 m below the mine level. The second choice may have corresponded to the true first arrivals at stations 2 and 13; however, these phases were so small that they could not be observed at stations 1 and 7.

The Vp/Vs ratio was 2.4 in the layer and 1.8 in the half-space of our model. A value of 1.8 is typical of most well-consolidated rocks; however, 2.4 is normal for shales, which comprise much of the layer.

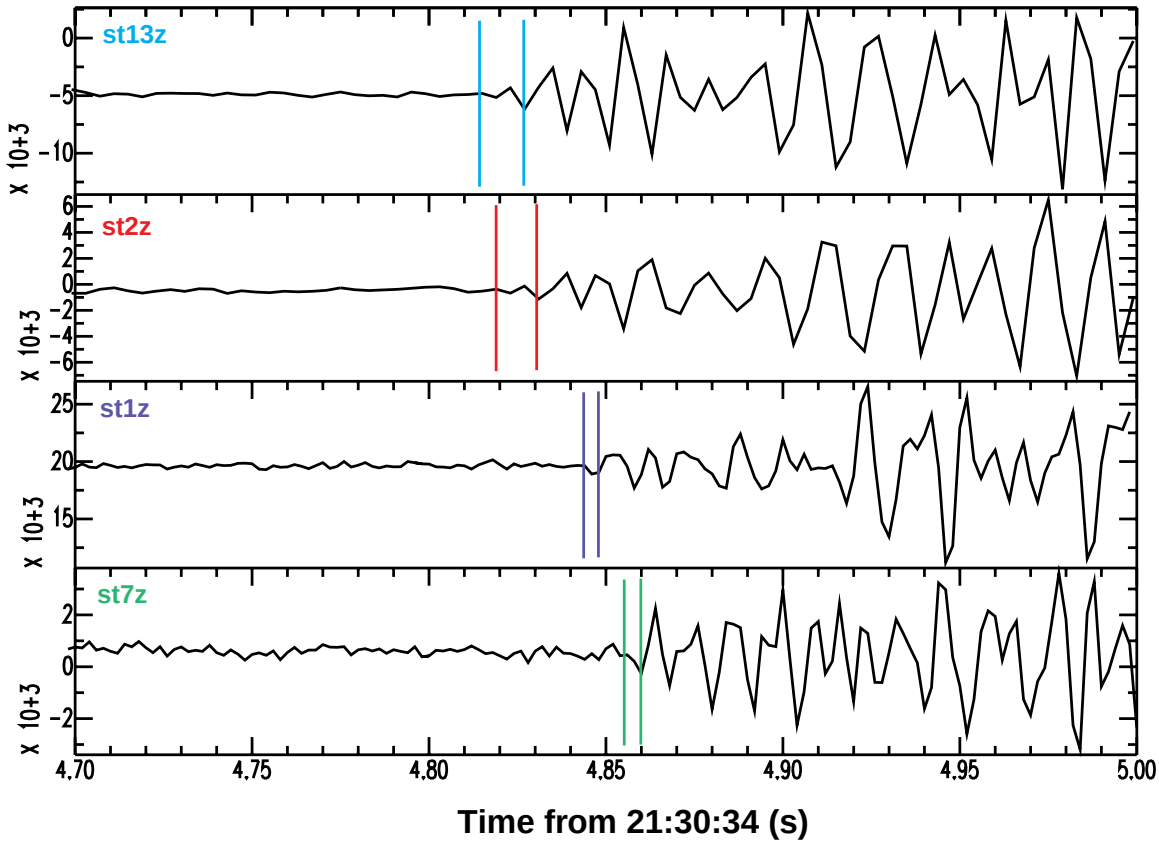

Figure 22. Pillar-shot, vertical-component seismograms at four close-in stations. Vertical bars show arrival times used in the calibration procedure.

P- and S-wave arrival times were determined manually for all aftershocks detected by a minimum of three stations by displaying vertical, radial and transverse components of motion. Radial and transverse components were obtained by rotating to the direction of ground zero. Arrival time estimates for a location directly beneath station 13, depth 318 m, helped to clarify multiple events. Arrival times and qualities assigned during processing were determined for all aftershocks that could be located. Qualities ranged from 0 to 4, only 0 and 1 were to be used in locating the event. A histogram of the number of P, S and total arrival times, quality 0 or 1, per event is shown in Figure 23a-c. The distributions peaked at 4 P, 4 S and 8 total arrival times per event.

We also plotted the percentage of quality 0 or 1 P and S arrival times at each station in Figure 24 a and b. High-quality data rates were 70% or so for the three innermost stations (within 300 m of ground zero), for both P and S waves. Rates drop to 30% at intermediate distance stations (600 m from ground zero) and to 10% or so at the outermost stations (>1000 m). We obtained microearthquake locations using an iterative, damped-least-squares (Geiger's) method. Arrival times were weighted by 1/T, where T was 4 ms for P waves and 12 ms for S waves. These values were our estimates of arrival time errors. Because initial results yielded a few large residuals (the difference between calculated and

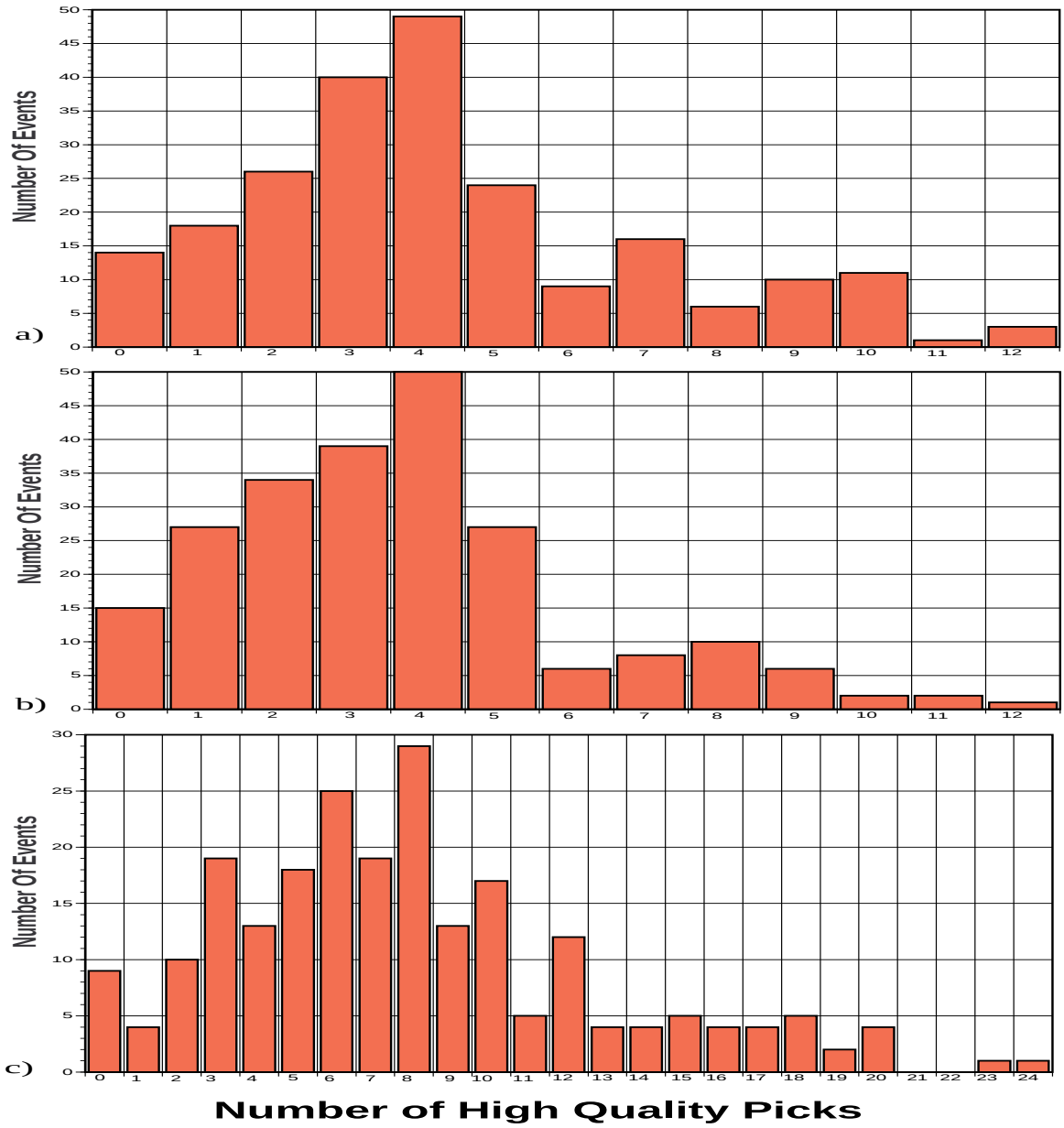

Figure 23. Histogram showing the number of aftershocks yielding high-quality (0 or 1) arrival times for a) P waves, b) S waves and c) total. Only 0 and 1 quality data were used to locate aftershocks.

observed data), we added a reweighting scheme. A weight remained the same if the associated residual's absolute value was less than T. Outside this range, weights decreased by a factor of T^2/R^2, where R was the residual. The form of the weight factor was chosen arbitrarily but should have little effect on the location results. The location calculation also included an estimate of the standard error ellipsoid, using the T's as the data error estimates.

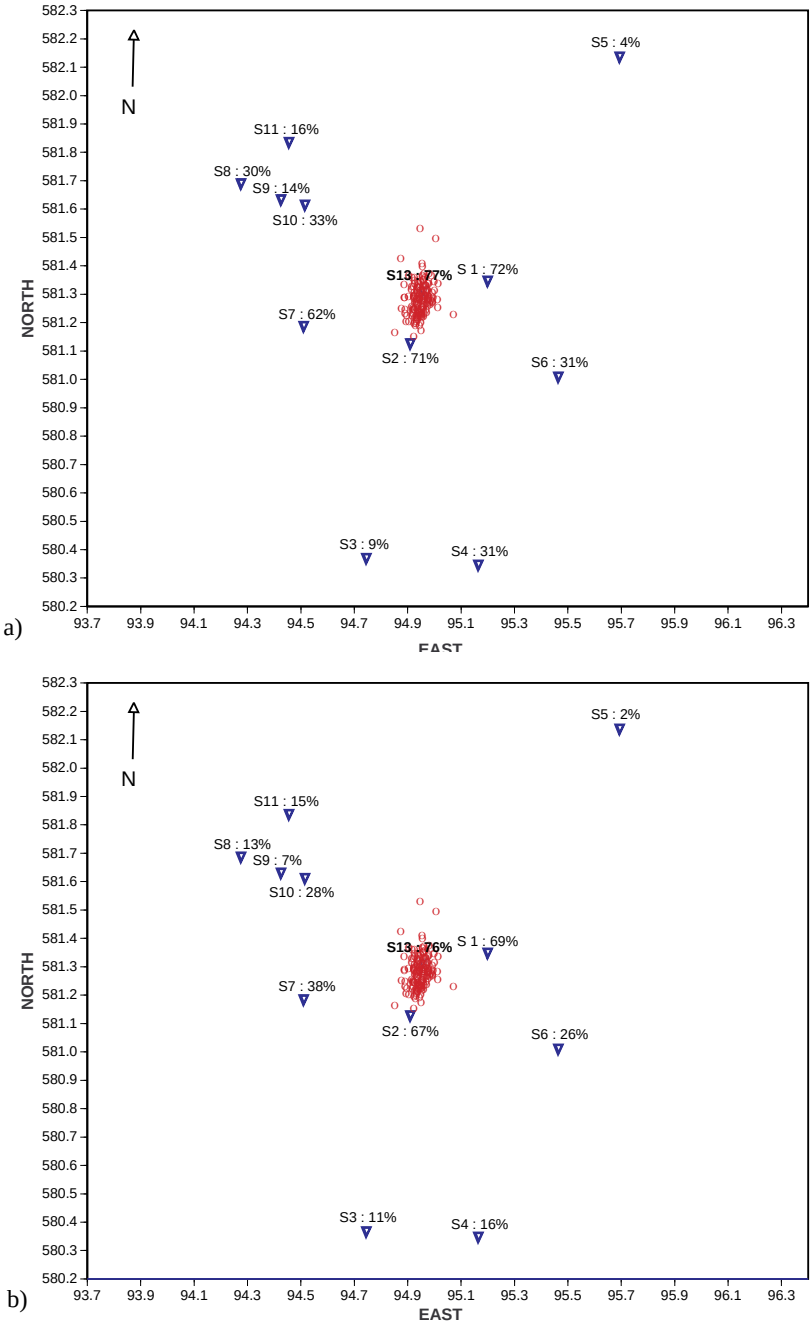

Figure 24. Map showing the number of high-quality (0 or 1) arrival times recorded at each station: a) P waves and b) S waves.

Aftershock Location Results

Plan and cross-section views of 135 aftershock locations are shown in Figure 25. These aftershocks were required to have 6 or more arrival times, largest error ellipsoid axis less than 50 m and RMS arrival time residual less than 7 ms.

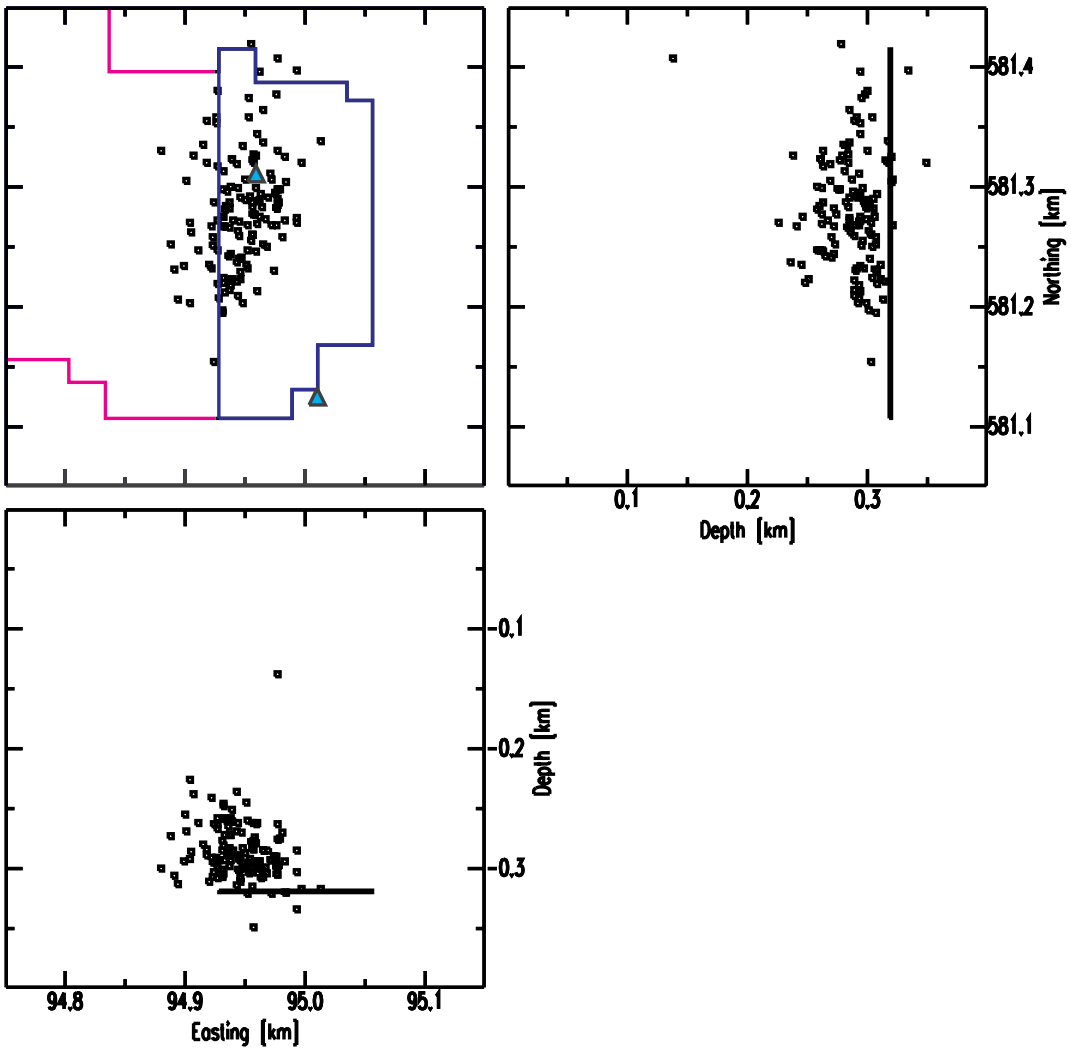

Figure 25. Map and cross-section views of aftershock locations. The map-view pink line represents the room-and-pillar mined area, the purple line encircles the collapsed panel. Triangles represent nearby stations. The collapsed panel is indicated by solid lines in the cross-section views.

Largest error axes generally pointed in near-horizontal directions as shown in the stereo plot of Figure 26. The aftershock plan view shows a distribution that fell short of the unmined faces of the mine by 50 m in places. However, the aftershocks lined up along the boundary between explosively collapsed and unaltered pillars on the western, open edge of the collapsed panel. The cross-section views show an aftershock zone just under 100 m thick, bottoming at mine level. In the cross-section view to the north, the distribution is asymmetrical, with the shallowest aftershocks falling closer to the open, western edge of the collapsed panel.

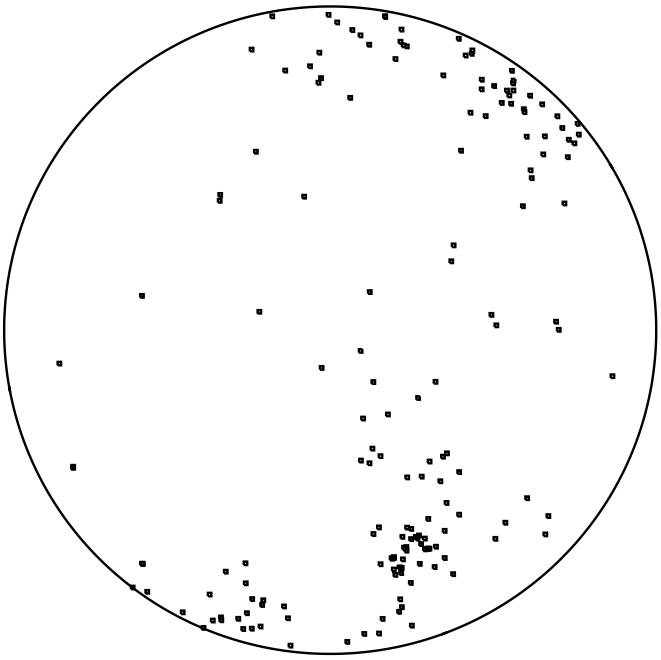

Figure 26. Orientation of major axes of error ellipsoids of aftershock locations, lower hemisphere projection.

To test the effectiveness of a smaller array of stations, we located aftershocks using data from innermost stations 1, 2 and 13 only. The resulting plan and cross-section views are shown in Figure 27. Although fewer events were located, distributions were similar to results using all stations and included some additional detail. Linear features can be seen in the cross-section view to the west. The western edge at mine level appeared surprisingly inactive in the cross-section view to the north.

After dividing events into time clusters defined in Figure 14, we determined that there was no change in the aftershock distribution with time. The only hint of space-time behavior were the linear features in the three-station locations, within which, many events occurred close together in time.

Discussion

The length of the first upward pulse of the collapse, acceleration signal shown in Figure 28 is related to the time of free-fall of material above the mine workings. If the rooms are 2 m in height, free fall should take roughly 0.6 s. The free-fall time indicated by the seismograms is 0.3 s or less, indicating a shorter fall of 0.5 m, presumably because of the rubblized pillars and bulking of fractured material from the mine back.

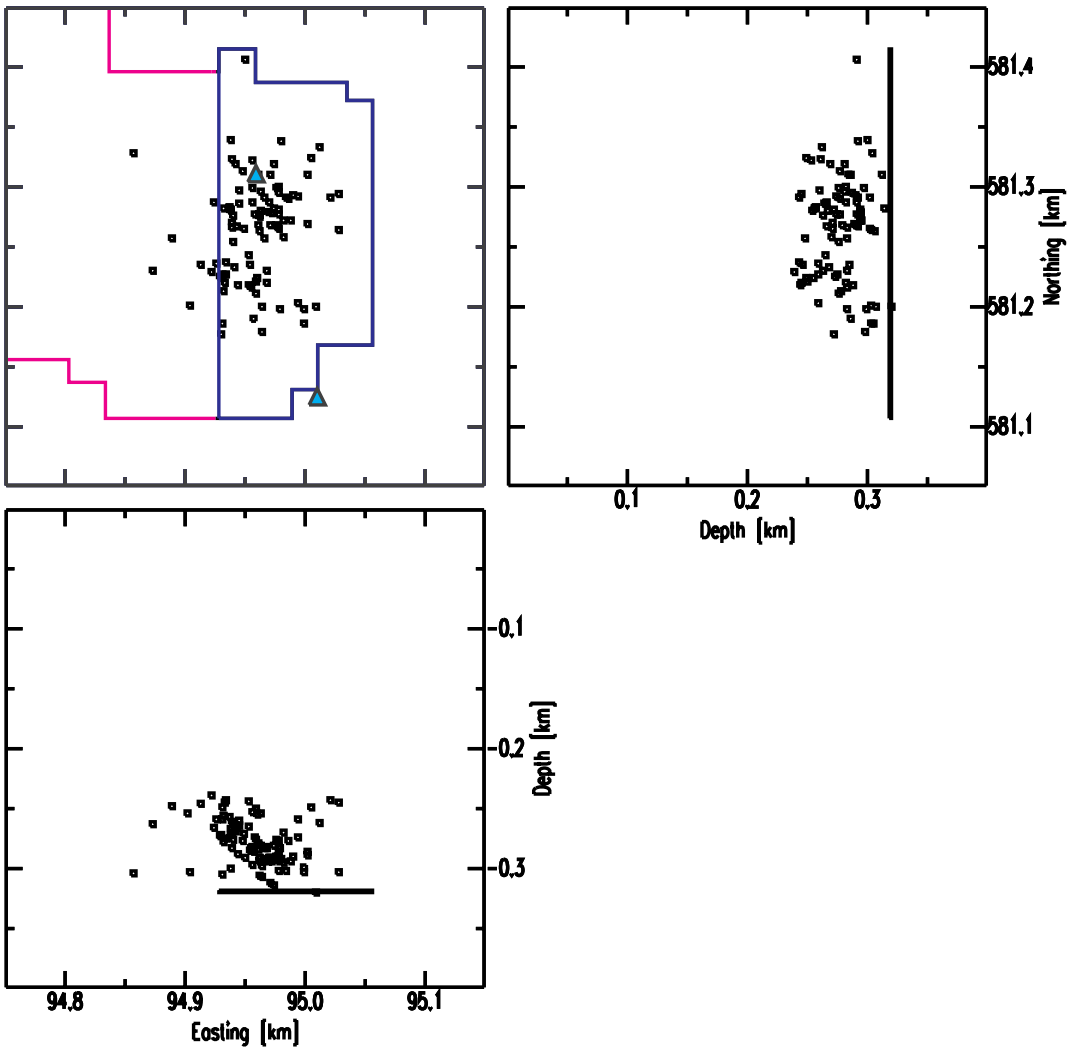

Figure 27. Map and cross-section views of aftershock locations obtained using data from stations 1, 2 and 13.

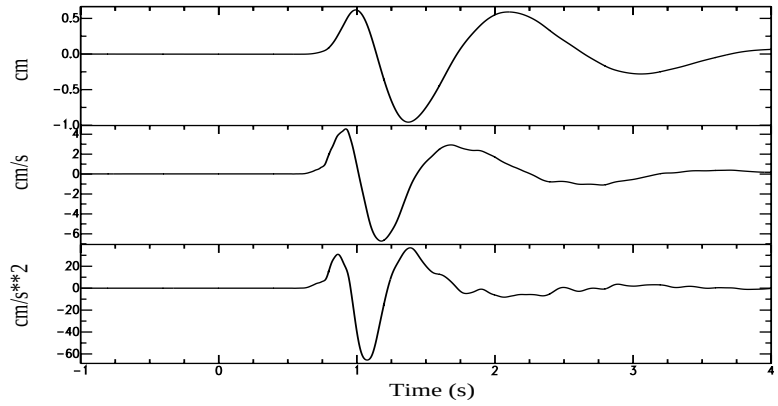

Figure 28. Instrument-corrected, vertical-component displacement, velocity and acceleration at station 13 during the collapse. Signals were low-pass filtered at 5 Hz.

Signal from the free-fall unloading was weak at regional distances (Figure 12). Although preceded by emergent motion, the strongest motion was up, associated with the slap-down phase of the mine collapse. While the slap-down phase produced downward motion at ground zero (station 13, Figure 28), regional ray paths would have left the source region in the downward direction, producing upward motion at regional distances.

Following Taylor, 1994, for a magnitude of 3.1 we calculated the mass of falling material to be $5.6X10^8$ kg. We assumed a free-fall distance of 0.5 m calculated from the ground-zero acceleration signal. Taking the aftershock zone as an estimate of the collapse area ($2X10^4$ m^2), a density of 2.5 gm/cm^3 and assuming uniform thickness of displaced material gave a thickness of 11 m. Magnitude, free-fall distance and area were chosen to overestimate mass and thickness. We used a New England coda scale which should overestimate magnitudes in north-central U.S. The free-fall distance was a fraction of the room height, accounting for pillar rubblization and bulking of displaced material from the mine back. Whether seismically inactive back edges of the panel actually collapsed or were supported by intact rock is indeterminate.

Aftershock activity decayed quickly after the collapse, 90% occurred in the first 4 hours. Thus, the refinement of a regional location for discrimination purposes by deploying a local array would be difficult because of the mobilization time required. The largest aftershocks were two orders of magnitude smaller than the main shock, making it unlikely that aftershocks would be recorded regionally. The aftershock zone was just under 100 m thick, the top of the zone lying over 200 m below the surface, the bottom at mine level. One stray, shallow event which barely passed the error test, was one of the few events with largest error axis oriented nearly vertical and had no data from station 13 at ground zero. This event location can be safely disregarded. Therefore, aftershocks gave no evidence that deformation related to the collapse approached the near-surface aquifer.

Stress on pillars adjacent to the collapsed panel was measured *in situ* and compared to models by Golder Associates (Forsyth, 1995). Models assumed a so-called unstressed region directly above the collapse, defined as any material whose load was supported through the rubblized zone rather than through the adjacent pillars or unmined faces. The thickness of the unstressed zone was estimated to be 110 m by projecting a 60 degree angle from the edges to the middle of the short span (east-west). This Golder model produced post-collapse stresses on adjacent pillars that matched well with measurements, except for the pillars immediately adjacent to the collapsed panel (first row) where measured stresses were lower than model predictions. If most aftershock slips are thrusting motions (horizontal convergence) as hinted by the distribution of first motions (Figure 15), aftershocks may be caused by a decrease in vertical stress relative to horizontal stress following the collapse. Thus, the aftershock zone may be related to the unstressed zone used in modeling. The vertical thickness of the aftershock zone was nearly the same as the assumed unstressed zone. However, asymmetry in the aftershock zone in the cross-section view looking north indicated more extensive (shallower) deformation adjacent to the open, western panel edge. In addition, the three-station locations indicated an inactive region, perhaps a thick rubble zone at mine level along the western edge. If the unstressed zone was modified to mimic the aftershock distribution, stress would be relieved along the western edge of the collapsed panel, enabling stress measurements in the first row of pillars to be matched more closely.

Locating aftershocks using the three stations closest to ground zero worked remarkably well. Although fewer events were located, more detail could be seen inside the active region. Data from distant stations may have added noise, loosing some detail in the full data set location patterns.

Conclusions

The explosively induced collapse of a panel in an underground room-and-pillar mine indicated that this type of controllable event will generate seismic signals which will propagate to at least near regional distances (as great as 1000 km). Magnitude was estimated to be 3.1 at most. Findings by the mining personnel indicated that the event behaved as planned and further work in the pillar rubblization pilot project will proceed.

Near-source monitoring of the mining collapse showed that the observed ground motion agreed well with previous work on mining collapses. The individual explosive charges emplaced in the pillars did not produce strong seismic signals, however, the failure of the pillars and the material above the working level did produce strong seismic signals. The strongest phase seen at regional distances was upward motion associated with the slap down of displaced material. We estimated upper bounds on mass, $5.6X10^8$ kg, and thickness, 11 m, of the displaced material.

Aftershocks that occurred following the collapse were at least 2 orders of magnitude smaller in amplitude than the ground motion generated by the collapse. The frequency of occurrence of the aftershocks decayed rapidly following the collapse. Of the located events, 90% occurred in the first 4 hours. These two observations argue that it would be difficult to use aftershocks to improve the location determined by regional observations.

Aftershock locations defined a zone of stress redistribution and deformation following the collapse. The bottom of the zone fell at mine level, the top over 200 m below the surface, offering no evidence of deformation extending to the near-surface aquifer. Deformation was more extensive (shallower) near the western, open edge of the collapsed panel, consistent with the low stresses measured in the first row of pillars, relative to stresses predicted by post-collapse models.

Recommendations

We can learn much about the main collapse through modeling efforts that include near field radiation and evaluate the effects of bulking.

Because stresses above the collapse are an important aspect of interpreting and modeling the effect on the surrounding pillars, we recommend a study of the focal mechanisms of aftershock events. This will involve a moment-tensor type calculation, because aftershocks were consistently recorded by only a few (3 to 5) of the close-in stations. The stress field as well as fracture patterns can be inferred from the results.

For future aftershock array deployments we recommend the following:

1. A tighter distribution of stations, covering an area no greater than one mine depth (300 m in the current case) from the edge of the panel to be collapsed, especially when the panel is surrounded by unmined faces.

2. Continuous recording, preferably at 500 samples/s for a period of 4 hours. The time length may have to increase for larger collapses. Recorders could be switched to trigger mode after this point to capture any later, swarm activity that might occur.

3. A well-coupled calibration shot with precise zero time. More than one shot location may be useful if the collapse panel is large. The pillar shots described in this report were barely sufficient for calibration purposes.

4. An underground seismometer. Presumably, GPS timing will not be available. If the internal clock fluctuates slowly, we can solve for time corrections. The underground seismometer will be useful for detecting smaller aftershocks, calculating statistics such as b-value and will sample raypaths that will be poorly recorded at the surface which will aid in determining focal mechanisms as well as locations.

5. Additional information such as depths of geological interfaces in the study area and velocity information from reflection surveys done by Geosphere Inc.

Acknowledgments

The success of our study was due, in great measure, to information provided by White Pine Mine personnel including reflection profiles and access to recording the shot break signal. We are grateful for their assistance.

References

Chaplin, M.P., S.R. Taylor and M.N. Toksoz, A coda-length magnitude scale for New England, *Earthquake Notes, 51*,15-22, 1980.

Forsyth, W., Modeling results for Unit 43 test panel, report to Copper Range Company, Golder Associates Ltd., October 1995.

Geosphere, Inc., Seismic reflection survey for northeast mine expansion planning, White Pine mine, report to Copper Range Company, May 1995.

St. Don, D.A., Pillar rubblization project, 70 pillar blast, internal report, Copper Range Company-Solution Mining Study, October 1995.

Singh, S. and R.B. Herrmann, Regionalization of crustal coda Q in the continental United States, *J. Geophys. Res., 88*, 527-538, 1983.

Taylor, S.R., False alarms and mine seismicity: An example from the Gentry Mountain mining region, Utah, *Bull. Seism. Soc. Am., 84*,350-358, 1994.